6

Imaging laser absorption spectroscopy of the metal-halide lamp under hyper-gravity conditions ranging from 1 to 10g

Abstract.
The metal-halide (MH) lamp shows an unwanted non-uniform distribution of the metal additive (Dy in our case), caused by convection and diffusion phenomena. MH lamps with various Hg pressures and burner lengths have been investigated by imaging laser absorption spectroscopy under varying gravity conditions in a centrifuge (1–10g). 2D ground state Dy density profiles have been determined. From these images, the density inhomogeneity and corrected axial segregation parameters are obtained. The profiles and parameters are affected by the axial temperature gradient, which is more pronounced for higher Hg pressures and shorter burner lengths.

This chapter has been adapted from [A.J. Flikweert, A.F. Meunier, T. Nimalasuriya, G.M.W. Kroesen and W.W. Stoffels, *Imaging laser absorption spectroscopy of the metal-halide lamp under hyper-gravity conditions ranging from 1 to 10g*, J. Phys. D: Appl. Phys. **41** (2008) issue 18].

6.1 Introduction

The metal-halide (MH) lamp is a high intensity discharge lamp with a good colour rendering and a high luminous efficacy [3, 21–26, 35, 39, 42]. MH lamps are for instance used for street lighting, stadium lighting, city beautification and shop lighting.

The lamp contains a buffer gas (usually Hg) and metal additives dosed as metal-halide salts (in our case DyI_3). The additives improve the colour rendering of the lamp. When the lamp is burning in the vertical position, axial colour segregation appears. The non-uniform light output limits the applicability, because it has a negative influence on the efficiency and the colour rendering of the lamp.

The non-uniform distribution of additives is caused by the combination of convection and diffusion in the lamp. The axial segregation of the additives has been described by E. Fischer [28]. An extension of this model has been proposed for our lamps in chapter 5 [73].

Convection is induced by gravity. In the past several experiments under varying gravity conditions have been carried out. Beside lab experiments [32, 34, 35, 50], the lamp was sent to the International Space Station ($0g$, where g is the gravity at earth: 9.81 m s^{-2}) [41]. Furthermore parabolic flights where carried out (0–$2g$, for periods of about 20 s; chapter 3 [33]). More recently a centrifuge was built, which can achieve gravity conditions from 1 to $10g$ (chapter 4 [37–39]). The additive distribution in the lamp, in our case the two-dimensional column density of ground state dysprosium atoms in a COST lamp [27], is measured by means of imaging laser absorption spectroscopy (ILAS) in chapters 4 and 8 [37, 39].

The aim of this chapter is to understand the flow phenomena in the lamp by studying the additive density distributions. The competition between convection and diffusion is understood by applying the recently developed semi-empirical axial segregation model [73].

In this chapter, first the theory of the axial segregation in the lamp is described briefly. Next we propose some parameters to characterize the lamp. The ILAS setup is discussed briefly. We show some 2D ground state atomic Dy density profiles. As an example two column density profiles are inverted to radial profiles by means of Abel inversion. Further analysis is done on the lateral density profiles. The 2D density distribution in the lamp is characterized by various parameters. For different lamp configurations (different length, different amount of Hg filling) the values for the ground state atomic Dy density inhomogeneity and the corrected axial segregation parameters are calculated from the ILAS results. Finally some conclusions are drawn.

6.2 Theory

The flow phenomena of the MH lamp have been described in the previous chapters [28, 32, 33, 67, 73]. First the theory of axial segregation is repeated briefly. The Abel

inversion technique, which is used to invert column density profiles into radial density profiles, is discussed briefly. Next the parameters that are used to characterize the ground state atomic Dy density profiles in the lamps are introduced.

6.2.1 Axial segregation

The temperature gradient between the hot centre ($\sim$ 5500 K) and the cooler wall ($\sim$ 1200 K) causes convection. The hot gas in the centre moves upwards, whereas the cooler gas at the wall moves downwards. Secondly, we have diffusion. At the wall mainly DyI_3 molecules are present. From the wall to the centre the molecules dissociate into atoms and in the very centre the Dy atoms are ionized to Dy^+. The diffusion of atoms and ions towards the wall is faster than the diffusion of the molecules towards the centre; this is called radial segregation. While the atoms are moving outwards and being associated into molecules, they are dragged downwards by convection. In this way Dy in any chemical form stays at the bottom of the lamp: the highest elemental Dy density is found at the bottom. This effect is maximal when the convection and diffusion are in the same order of magnitude: maximal axial segregation appears. In the limiting cases, when no convection is present or when the convection is very strong (e.g. hyper-gravity), good axial mixing occurs.

Besides the convection and diffusion, another process determines the atomic Dy density distribution. The temperature determines the chemical equilibrium between molecules, atoms and ions. In our lamps, we have an axial temperature gradient. The axial segregation is determined not only by convection and diffusion but also by the axial temperature profile [73]. This axial temperature gradient determines the 2D density profiles, the axial density inhomogeneity and the accuracy of the corrected Fischer parameter.

6.2.2 Abel inversion

The column density profile gives the line-integrated density at each lateral position (x, z). Because the plasma is radially symmetric, one would like to invert the lateral profile $n_{\mathrm{col,Dy}}(x, z)$ (m^{-2}) into a radial profile $n_{\mathrm{Dy}}(r, z)$ (m^{-3}). The column density profile can be inverted to a radial density profile by means of Abel inversion [29, 32, 34, 41, 49, 64]. The column density at lateral position x and the axial position z is given by

$$n_{\mathrm{col,Dy}}(x, z) = 2 \int_x^R \frac{n_{\mathrm{Dy}}(r, z)}{\sqrt{r^2 - x^2}} r dr, \tag{6.1}$$

where $n_{\mathrm{Dy}}(r, z)$ is the radial density and R is the radius of the burner. The radial density profile can be estimated by a polynomial series (e.g. $a_n r^n$ or Legendre polynomials). Other methods are filtered backprojection by using fast fourier transform and onion peeling [48, 63, 74, 75]. By onion peeling, first the density of a ring at the edge

of the plasma is determined. Next this is ring is subtracted, and the density in the next ring is determined, and so on until the density at the centre is determined. An accumulation of small errors at the edge is thereby translated into larger errors at the centre.

Zhu [29] performed numerical tests of the Abel inversion using polynomials. This Abel inversion method is sensitive to noise in the column density data, especially at the centre. A bit of noise gives a totally different radial profile; different radial profiles correspond to almost the same lateral profile.

These Abel inversion techniques are too complicated and are sensitive to noise. For this reason, we use a simple Abel inversion technique. We assume a simple radial profile $n_{\mathrm{Dy}}(r,z)$. A drawing is given in figure 6.1. The profile consists of $N = 16$ concentric rings with a constant density a_i within ring i. The advantage of this profile is that all rings can be forced to be positive. The density is given by

$$n_{\mathrm{Dy}}(r,z) = a_i \quad \text{where} \quad i = \mathrm{floor}\left(\frac{r}{R}N + 1\right). \tag{6.2}$$

In the lateral domain we obtain

$$n_{\mathrm{col,Dy}}(x,z) = \sum_{i=1}^{N} a_i \cdot d(x,i)\ , \tag{6.3}$$

where

$$d(x,i) = \begin{cases} 2\left(-\sqrt{r_1^2(i)-x^2} + \sqrt{r_2^2(i)-x^2}\right) & \text{for } 0 \le x < r_1(i) \\ 2\sqrt{r_2^2(i)-x^2} & \text{for } r_1(i) \le x < r_2(i) \\ 0 & \text{for } x \ge r_2(i) \end{cases} \tag{6.4}$$

and

$$\begin{aligned} r_1(i) &= \tfrac{i-1}{N}R, \\ r_2(i) &= \tfrac{i}{N}R. \end{aligned}$$

Fitting the values a_i in the lateral domain (equation (6.3)) gives the radial profile $n_{\mathrm{Dy}}(r,z)$ (equation (6.2)). The constraint is that all a_i have positive values.

6.2.3 Parameters

Various parameters describe the density distribution of Dy atoms in the lamp. The axial segregation can be described by the density inhomogeneity and the axial segregation parameter. These parameters have been described in chapter 5 [73] and are summarized here.

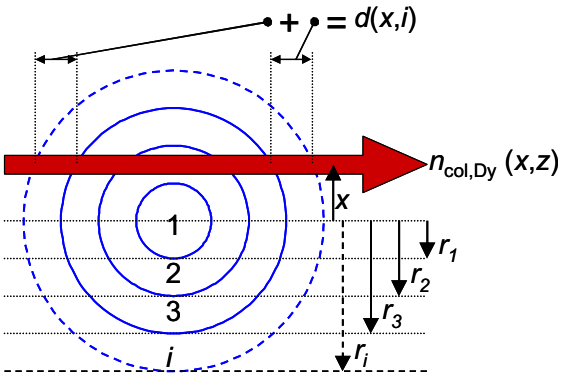

Figure 6.1: Schematic drawing of the cross-section of a cylindrical symmetric plasma at the axial position z. For Abel inversion, we assume concentric rings of constant density a_i. The radii of the rings are indicated by r_i. The column density $n_{\mathrm{col,Dy}}(x,z)$ in this example consists of contributions from ring 2 to i. The distance $d(x,i)$ travelled through ring i is also indicated.

Density inhomogeneity

The inhomogeneity of a lamp property $Q(z)$ was introduced in equation (5.10). In this chapter the inhomogeneity of the ground state atomic Dy density integrated over the cross-section at the axial position z is derived; $Q(z) = N_{\mathrm{Dy}}(z)$ (m^{-1}). The axial density inhomogeneity gives a measure for how non-uniform the distribution of ground state Dy atoms over the lamp height is, analogous to equation (5.10):

$$\alpha = \sqrt{\frac{1}{H}\int_0^H \left(\frac{N_{\mathrm{Dy}}(z) - \overline{n}_{\mathrm{Dy}}}{\overline{n}_{\mathrm{Dy}}}\right)^2 \mathrm{d}z}, \tag{6.5}$$

where H is the height of the lamp burner. A value of $\alpha = 0$ means that the Dy atoms are evenly distributed over the height of the lamp. The parameter is normalized for the lamp height and the average density $\overline{n}_{\mathrm{Dy}}$.

The density per unit length of the lamp $N_{\mathrm{Dy}}(z)$ can be obtained by integrating the radial density profile over the radius of the lamp. This is equal to integrating the column density profile over the width of the lamp:

$$N_{\mathrm{Dy}}(z) = \int_0^R n_{\mathrm{Dy}}(r,z)\cdot 2\pi r \mathrm{d}r = \int_{-R}^R n_{\mathrm{col,Dy}}(x,z)\mathrm{d}x. \tag{6.6}$$

The density inhomogeneity is determined by the axial segregation (following section) and the axial temperature profile in the lamp.

Axial segregation parameter

To compare with earlier measurements where Fischer parameters were obtained, a corrected Fischer parameter has been introduced in equation (5.13) which takes the temperature influence into account. The Fischer formula of the Dy density N_{Dy} as a function of the axial position z is given by [28, 73]

$$N_{\mathrm{Dy}}(z) = N_{\mathrm{Dy},0} \cdot \exp\left(-\lambda z\right). \tag{6.7}$$

When we take the temperature influence into account, the radially integrated atomic Dy density is given by:

$$N_{\mathrm{Dy}}(z) = N_{\mathrm{Dy},0} \cdot \exp\left(-\lambda_{\mathrm{c}} z\right) \cdot \left(1 - \exp\left(-a\left(z-b\right)^2\right)\right) \cdot \left(1 + cz\right). \tag{6.8}$$

In this equation, $N_{\mathrm{Dy},0}$ is the atomic Dy density at the bottom of the lamp burner per unit length (m^{-1}), and the radially integrated atomic Dy density $N_{\mathrm{Dy}}(z)$ is the amount of atomic Dy per unit length (m^{-1}) present in the cross-section at the axial position z [73]. Fitting this equation from the measured $N_{\mathrm{Dy}}(z)$ yields the fitting parameters a, b and c which take the temperature variation along the axis into account, and the corrected axial segregation parameter λ_{c}. This parameter, λ_{c}, is determined by the ratio of the amount of convection and diffusion. Convection increases with Hg pressure, radius and gravity, and decreases at increasing input power [28, 33, 37].

6.3 Experimental setup

Five lamps have been investigated under hyper-gravity conditions (1–10g). The goal of this study is to compare the various lamps, and to investigate the axial Dy distribution as a function of the amount of convection.

6.3.1 Lamps

The lamps we use are COST reference lamps (section 1.3.1) [27]. A drawing is given in figure 6.2. The diameter of the lamp burner is 8 mm and the burner height is 14–20 mm. The electrode distance is 8 or 16 mm. The lamps contain various amounts of Hg as buffer gas and contain DyI_3 as salt additive. The specifications of the lamps are given in table 6.1. For the calculation of the pressure an effective temperature of $T_{\mathrm{eff}} = 3000$ K is assumed [33, 53].

Due to deterioration of the lamp, some deviations from the predicted values can be observed. Chemical analysis after x-ray fluorescence measurements by Nimalasuriya *et al* [38] show that during lamp operation Dy is being removed by chemical reactions at the wall, leaving an excess of free iodine. Before we started the measurements, lamps 1 and 3 had been operated for a longer time than lamp 2. Thus more deterioration is expected for these lamps 1 and 3.

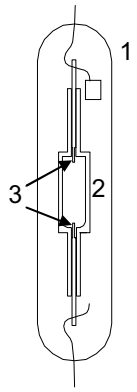

Figure 6.2: Schematic drawing of the lamp [37]: (1) outer bulb; (2) burner (diameter 8 mm, height between 14 and 20 mm); (3) electrodes (distance 8 or 16 mm).

Table 6.1: Lamp specifications. The diameter d and height h refer to the inner wall of the burner. When the cold zones behind the electrodes are taken into account, the pressures are about 20%–30% lower.

Lamp no.	d (mm)	h (mm)	Electrode dist. (mm)	Hg (mg)	DyI_3 (mg)	p_{Hg} (∼bar)	P (W)
#1	8	20	16	5	4	6	109.5, 129.9, 148.4
#2	8	20	16	7.5	4	9	109.5, 129.9, 148.4
#3	8	20	16	10	4	12	109.5, 129.9, 148.4
#4	8	15.5	8	6	4	10	89.5
#5	8	14	8	12	4	21	89.5

6.3.2 Centrifuge

As explained in sections 6.1 and 6.2.1, convection depends on gravity. A centrifuge was built to investigate the lamp under varying gravity conditions [37, 67]. It consists of a pivot, an arm and a gondola connected to the arm. The centrifuge has a diameter of about 3 m. The maximum rotation frequency is ~ 1.5 Hz, corresponding to $10g$ at the lamp position; g is the gravity on earth (9.81 m s^{-2}). The gravity vector at the lamp is always parallel to the lamp axis; the size of the vector parallel to the lamp axis is defined by a_z. The gondola contains the lamp and the setup. The measurement techniques are emission spectroscopy, webcam imaging and ILAS.

6.3.3 Measurement techniques

In this chapter, we present results of the ILAS measurements. ILAS yields the two-dimensional ground state atomic Dy column density. The ILAS technique has been discussed in chapter 4 and is summarized here.

A diode laser is used to scan over a wavelength range of ∼0.1 nm around the absorption wavelength of 642.19 nm of ground state atomic Dy. The laser beam is expanded so that it illuminates the whole lamp burner. Part of the laser light is absorbed by the Dy atoms in the lamp. After passing the burner, the laser beam is imaged on a CCD camera.

The wavelength scan is performed in 65 steps. For each wavelength step the transmission is calculated for each position (x, z) in the lamp burner. In this way, we obtain a 3D matrix (wavelength, lateral position x, axial position z) with transmission data. From the wavelength dependence a transmission curve is constructed for each position. Next the density is obtained from this curve. We thus obtain the Dy density for each position (x, z) and end up with a 2D ground state atomic Dy column density profile.

Compared with emission, with ILAS this density is obtained directly and also non-radiating particles are measured. This means that also colder regions of the lamp can be measured, where emission spectroscopy cannot detect Dy atoms. Note that by using ILAS only ground state Dy atoms are measured. The ratio between Dy atoms in all states and Dy atoms in the ground state ranges from 1 to ∼3 for 6000 K. This ratio β is given by the following semi-empirical formula based on the partition sum data of [76]:

$$\beta(T) = 0.815 + 0.0213 \exp\left(6.03 \times 10^{-4} \cdot (T + 2099)\right), \tag{6.9}$$

where the temperature T is in Kelvin.

The specifications of the ILAS technique are as follows. The spatial resolution is ∼10 μm. The minimum detectable column density is 10^{17} m^{-2}, which in our lamps corresponds to a density of 10^{19} m^{-3}. The measurement time for one 2D profile is about 10 min. The measurement time is determined mainly by the download time of the CCD images. During the measurement, the data are stored locally on the computer in the centrifuge gondola. After the measurement is finished, the data are downloaded from the centrifuge computer and processed off-line. After the 2D ground state atomic Dy density images have been constructed, further analysis can be performed and the parameters as described in section 6.2.3 can be obtained.

By using ILAS, lamps with DyI_3 can be measured. The diameter of the lamp burner is fixed at 8 mm because of the optical system. However, the height of the lamp burner can be varied to maximum 20 mm.

Besides ILAS, the lamp is monitored by a simple webcam. From these images the colour segregation in the lamps can be observed directly.

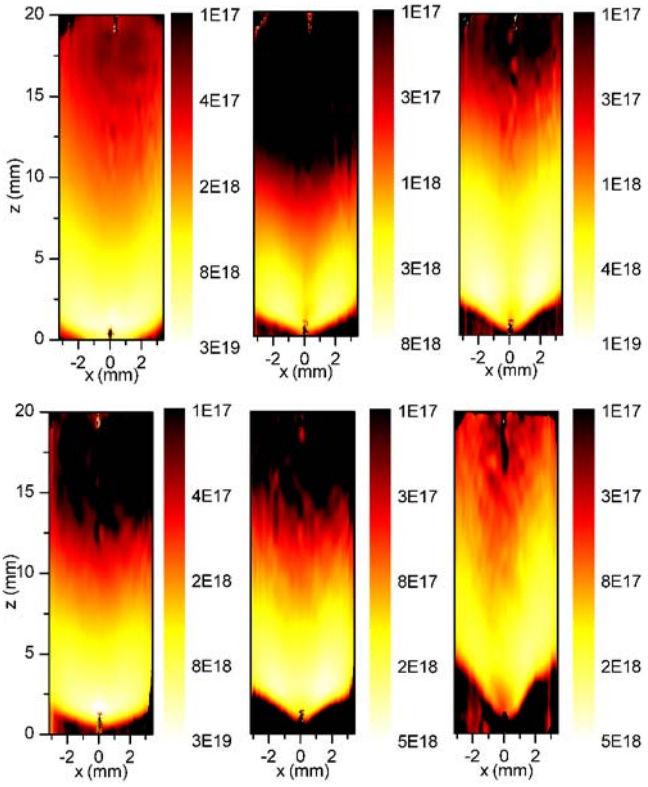

Figure 6.3: Lateral 2D ground state atomic Dy density profiles for the long lamps (20 mm burner length): lamp 1, 5 mg Hg ($1g$, $4g$ and $10g$) and lamp 3, 10 mg Hg ($1g$, $4g$ and $10g$), all at $P = 148.4$ W. The column densities are given in m^{-2}.

6.4 Results

Various lamps (different burner length, Hg pressure) under various input power have been investigated as a function of the amount of gravity. First, we show 2D column density profiles of ground state atomic Dy and discuss these in detail. In addition, webcam images are compared with the 2D profiles. Next two Abel inverted profiles are shown for lamp 1 (20 mm burner). The lamp numbers used in this section are given in table 6.1.

From the column 2D density profiles, several parameters are obtained as a function of gravity for the five lamps. For all lamps the values for the density inhomogeneity and the corrected axial segregation have been obtained for the power settings given in

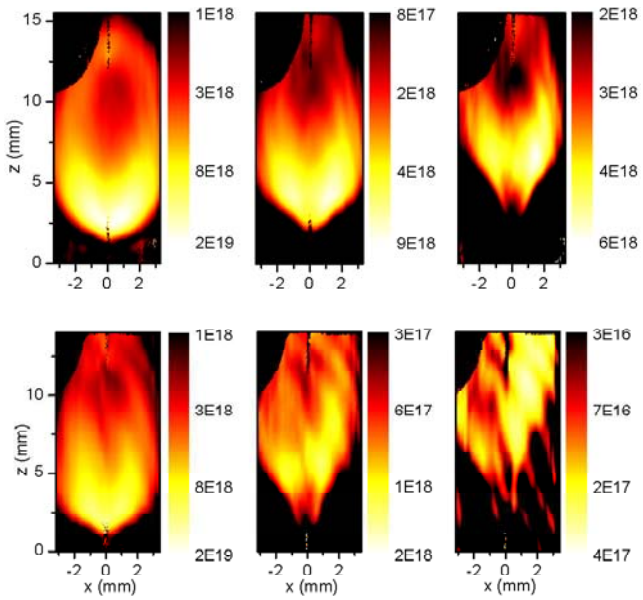

Figure 6.4: Lateral 2D ground state atomic Dy density profiles for the short lamps: lamp 4, 6 mg Hg ($1g$, $4g$ and $10g$) and lamp 5, 12 mg Hg ($1g$, $4g$ and $10g$), all at $P = 89.5$ W. The column densities are given in m^{-2}. The dark region at the top left is caused by an irregularity in the glass, which hinders the laser beam. Therefore no Dy atoms can be measured at this position.

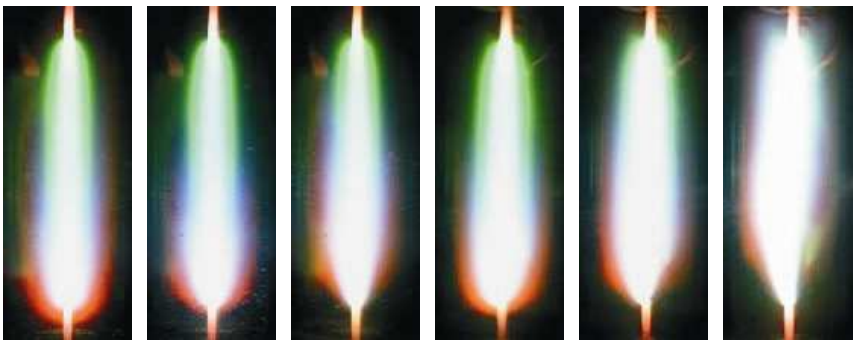

Figure 6.5: Webcam images for the long lamps: lamp 1, 5 mg Hg ($1g$, $4g$ and $10g$) and lamp 3, 10 mg Hg ($1g$, $4g$ and $10g$), all at $P = 148.4$ W.

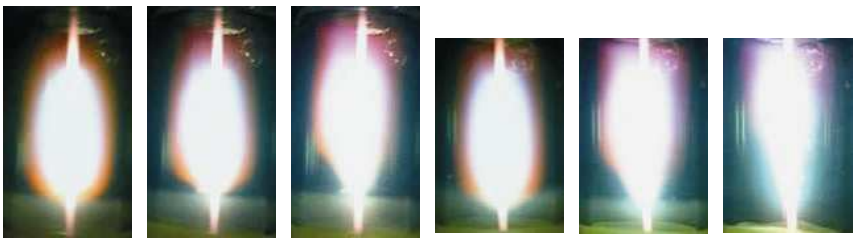

Figure 6.6: Webcam images for the short lamps: lamp 4, 6 mg Hg ($1g$, $4g$ and $10g$) and lamp 5, 12 mg Hg ($1g$, $4g$ and $10g$), all at $P = 89.5$ W. The irregularity in the glass at top right originates from the manufacturing process.

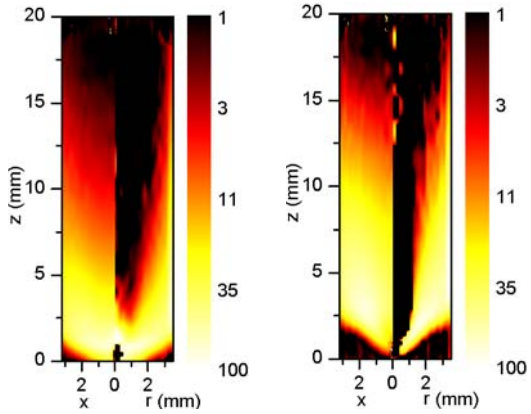

Figure 6.7: Abel inverted profiles lamp 1 (20 mm burner length), 5 mg Hg, 148.4 W: at the left side the lateral profile and at the right side the radial profile. The densities are in relative units on a logarithmic scale.
(left) $1g$, the lateral density scale ranges from 3×10^{17} to 3×10^{19} m^{-2} and the radial density scale from from 3×10^{19} to 3×10^{21} m^{-3}.
(right) $10g$, the lateral density scale ranges from 1×10^{17} to 1×10^{19} m^{-2} and the radial density scale from from 1×10^{19} to 1×10^{21} m^{-3}.

table 6.1. In this chapter, we focus on the trends of the gravity dependence of these parameters for different Hg pressures and input power.

6.4.1 2D profiles

Figures 6.3 and 6.4 show 2D profiles of ground state atomic Dy for the various lamps. Figures 6.5 and 6.6 show the webcam images for the lamps. The ground state atomic

Dy density at the top and the bottom of the lamp is too low to be measured (below the noise level). Therefore black parts are observed at the top and bottom of the lamp. The irregular flame-like pattern close to the top of the lamp is also caused by noise [37].

In the density profiles at the bottom no Dy atoms are present, caused by the low temperature. The arc angle at the bottom is defined by the angle between the visible arc and the bottom plane of the lamp burner. Because the axial temperature profile changes with gravity, the angle also changes with gravity. The arc angle is minimal at maximum axial segregation.

For lamps 1–3 (long, 20 mm burner) higher gravity means less segregation; better mixing is observed (right side of the Fischer curve [28, 73]). At $1g$ the ground state atomic Dy density is the highest at the spot around the bottom electrode. The electrode temperature is about 2800 K [70] and at this temperature the atomic Dy density is the highest [73] due to the chemical equilibrium. For lower temperatures the equilibrium shifts towards molecules, whereas at higher temperature the Dy atoms are ionized. At higher gravity the convection flow causes cooling in the region around the electrode and the local atomic Dy density is decreased. At the very bottom of the lamp the temperature is too low for Dy atoms to exist.

For lamps containing 5 mg Hg, the Dy density is higher than the lamp containing 10 mg. This is because at 10 mg the radiation loss by Hg atoms is larger, thus the temperature of the cold spot is lower than at 5 mg Hg. This causes a lower overall Dy density.

When we take a look at the short lamps 4 and 5, we see that above $3g$ the maximum white light output is observed at the top of the lamp. This is most pronounced for lamp 5. The Dy density is also the highest at the top. This is caused by the temperature effect (section 6.2.1 [73]), due to the strong convection. At the bottom the chemical equilibrium shifts from atoms to molecules, causing a smaller atomic Dy density.

For the short lamp lamp 5, the overall density at $10g$ is much lower than at $1g$ and $4g$, due to cooling by the strong convection. As stated in section 6.3.3, the detectable column density is about 10^{17} m^{-2}. The minimum value shown in the 2D profile is 3×10^{16} m^{-2}, but the image is noisy and some artefacts are seen. Nevertheless it is clear from this image that most of the atomic Dy is observed at the top of the lamp.

6.4.2 Abel inversion

The column density profiles can be inverted into radial profiles by means of Abel inversion as explained in section 6.2.2. As an example, the Abel inverted profiles are derived for lamp 1 (20 mm burner length). These profiles consist of 16 rings. Figure 6.7 shows these radial profiles together with the lateral profiles, for $1g$ and $10g$. At $10g$ better mixing is observed and the maximum density moves outward. In the centre almost no atomic Dy is present, because the temperature is too high and mainly ions are present.

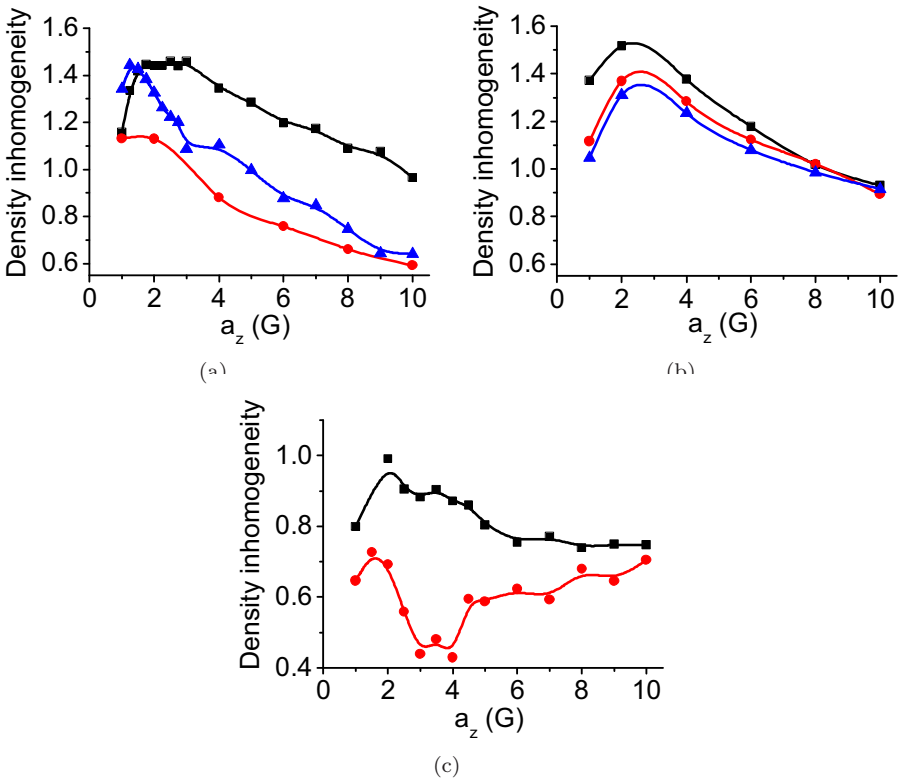

Figure 6.8: Density inhomogeneity α, as a function of the gravitational acceleration a_z. The lines are shown to guide the eye.
(a) 20 mm lamps, pressure series, 148.4 W: ■ lamp 1 (5 mg Hg); ● lamp 2 (7.5 mg Hg); ▲ lamp 3 (10 mg Hg).
(b) 20 mm lamp 1, input power series, 5 mg Hg: ■ 109.5 W; ● 129.9 W; ▲ 148.4 W.
(c) 15 mm lamps, pressure series, 89.5 W: ■ lamp 4 (6 mg Hg); ● lamp 5 (12 mg Hg).

6.4.3 Density inhomogeneity

The axial density inhomogeneity parameter is determined by the ratio between convection and diffusion and by the temperature effect (section 6.2.3). Figure 6.8 shows the density inhomogeneity α of ground state Dy atoms for various Hg pressures and for various power, as a function of gravity. The ratio between atomic Dy in the ground state and all states is given in equation (6.9). For the calculation only the part between $|x| = 0.5$–3.0 mm is taken into account, because of noise at the centre (electrodes) and close to the burner wall.

The density inhomogeneity should decrease with increasing Hg pressure, because the convection speed is proportional to the pressure. Our lamps are at the right-hand side of the Fischer curve, thus increasing the convection means decreasing the amount of axial segregation [28, 33, 37, 73]. The decrease is observed in figure 6.8(a); however, the values for the long lamps, 2 and 3 (20 mm burner length), are close to each other. The density inhomogeneity α should be smaller for lamp 3 than for lamp 2, because of the higher pressure. However, this is not the case. An explanation is that the temperature effect is more pronounced for lamp 3 than for lamp 2, increasing the density inhomogeneity for lamp 3 more than for lamp 2. Furthermore increasing the power results in increasing the convection speed [23, 73]. This causes the density inhomogeneity to decrease with increasing power; this is observed in figure 6.8(b).

The maximum density inhomogeneity shifts towards higher gravity for lower Hg pressure. The convection speed is proportional to $v \sim p_{\mathrm{Hg}}^2 g$. The axial segregation is determined by the ratio of the rate of convection to the rate of diffusion [28, 42, 73]. For a constant convection speed, the amount of gravity g should decrease when increasing the pressure. Furthermore the density inhomogeneity decreases with increasing gravity, because we are at the right-hand side of the Fischer curve.

At $1g$, the density inhomogeneity is lower for the short lamps 4 and 5 (figure 6.8(c)) than for the long lamps 1–3. At higher gravity, axial segregation is still present. The axial segregation (λ_{c} in equation (6.8)) is smaller (right side of the Fischer curve), but the temperature effect becomes dominant and cancels the smaller Fischer segregation. At $3g$, α is minimal for the short lamp 5. Thus at $1g$ the highest density is found at the bottom due to the axial segregation, and at $10g$ the highest density is found at the top due to the temperature effect. Around $3g$ the lamp is in between these two situations, giving the most homogeneous Dy distribution. This is in agreement with the 2D profiles (figure 6.4) and the webcam images (figure 6.6), where we see that above $3g$ the atomic Dy density is the highest at the top of lamp 5.

6.4.4 Corrected axial segregation parameter

In the density profiles (figures 6.3 and 6.4) it is observed that no ground state Dy atoms are present at the bottom of the lamp due to the low temperature. This causes the arc angle that is observed near the bottom. For this part in the lamp, no corrected axial segregation parameter λ_{c} can be fitted according to equation (6.8). The same arc angle can also be observed at the top of the lamp; also at this position no fit can be performed.

The solution to use a larger region for fitting the parameter is as follows. First the density plot is straightened by subtracting the contour line (defined at one-fifth of the maximum density) from the z coordinate. For the calculation of the contour only the part between $|x| = 1.0$–2.5 mm is taken into account. Next the corrected axial segregation parameter is fitted. This gives the same value for λ_{c} according to equation (6.8). In conclusion, the arc angle correction yields the same axial segregation

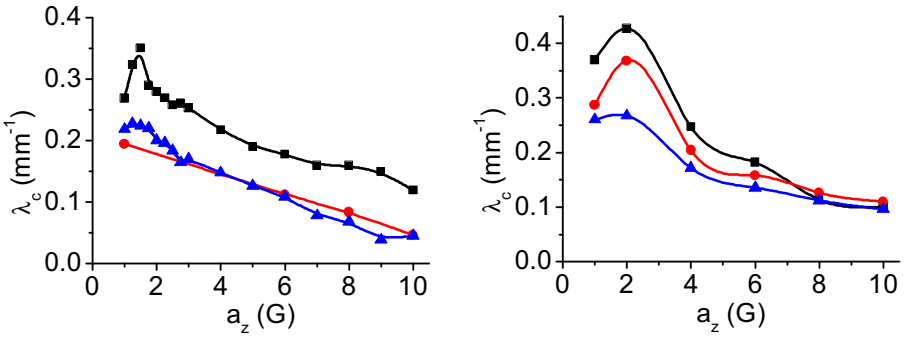

Figure 6.9: Corrected segregation parameter λ_c, as a function of the gravitational acceleration a_z. The lines are shown to guide the eye.
(a) 20 mm lamps, pressure series, 148.4 W: ■ lamp 1 (5 mg Hg); ● lamp 2 (7.5 mg Hg); ▲ lamp 3 (10 mg Hg).
(b) 20 mm lamp 1, input power series, 5 mg Hg: ■ 109.5 W; ● 129.9 W; ▲ 148.4 W.

parameter, but a larger z range of the lamp can be fitted.

In figure 6.9 the trends of the corrected axial segregation parameters λ_c are shown. The values differ from the uncorrected values as shown in the paper by Nimalasuriya *et al* [38], especially for higher gravity and for 10 mg Hg (lamp 3, long burner). The corrected values are at higher gravity lower than in [38] and are in closer agreement to the the $1/g$ dependence predicted by E. Fischer [28, 73]. Furthermore the segregation decreases more strongly with pressure than in the earlier publication.

The axial segregation decreases with increasing pressure (figure 6.9(a)). The curves also show a decrease in axial segregation when increasing the power (figure 6.9(b)). This is because increasing the power increases the temperature gradient and thus the convection speed. When we are at the right-hand of the Fischer curve, increasing the amount of convection means decreasing the amount of axial segregation.

In general, the corrected axial segregation and the square of the density inhomogeneity show the same dependence of pressure, gravity and input power. When the temperature effect is not dominant, λ_c and α^2 should follow the same trends. An example is given in figure 6.10, where these two parameters are compared for lamp 3 (20 mm burner length) at 148.4 W. These parameters show indeed good agreement with each other.

When figure 6.9(a) is compared with figure 6.8(a), it is observed that lamps 1–3 show a decreasing λ_c with increasing pressure, whereas for lamps 2 and 3 α increases with increasing pressure. The latter is explained by the stronger temperature effect for lamp 3, increasing the axial density inhomogeneity.

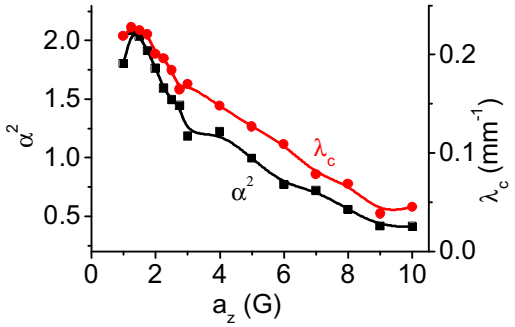

Figure 6.10: Comparison between the square of the density inhomogeneity (α^2) and the corrected segregation parameter λ_c for the long lamp 3, 10 mg Hg, 148.4 W, as a function of the gravitational acceleration a_z: ■ α^2 (left axis); ● λ_c (right axis). The lines are shown to guide the eye.

For the short lamps 4 and 5 the temperature effect is dominant. In this case, the density $N_{\mathrm{Dy}}(z)$ is governed mainly by the temperature (second) part in equation (6.8) and the fitting of the variable λ_c is inaccurate. Therefore, λ_c is not shown for these lamps.

In conclusion, the corrected axial segregation parameter is only valid if the temperature effect does not dominate. This corrected parameter follows the behaviour predicted by E. Fischer better than the uncorrected Fischer parameter.

6.5 Conclusions

MH lamps containing DyI_3 as salt additive have been measured by ILAS. 2D ground state atomic Dy lateral density profiles have been obtained for lamps with various Hg pressures, various burner lengths (20 mm and $\sim$ 15 mm) and various input power. The lamps have been measured in a centrifuge, which yields a gravity between 1 and 10g. The 2D density profiles have been compared with webcam images. For the shorter lamps ($\sim$ 15 mm burner length), at 10g the highest Dy density is found at the top of the lamp, caused by the strong axial temperature gradient.

As an example, two lateral density profiles have been inverted to radial profiles. The radial profiles show a dip of atomic Dy density in the centre.

From the 2D images, the density inhomogeneity and corrected axial segregation parameters have been derived. The axial segregation parameter was corrected for the temperature effect. For lamps with a burner length of 20 mm the corrected segregation parameter follows better the predicted behaviour by E. Fischer than the uncorrected parameter as used in an earlier publication. For short (height $\sim$15 mm) lamps the

temperature effect is dominant. Because of this, for the short lamp with high Hg pressure (12 mg) at $10g$ the highest density is found at the top of the lamp. If the temperature effect is dominant, the corrected segregation parameter is not relevant to describe the axial segregation in the lamp.

Acknowledgements

The authors are grateful to all participants in the ARGES project for their contributions, especially the General Technical Department of the Eindhoven University of Technology for building the centrifuge, and Senter-Novem (project EDI 03146), SRON [66] and the Dutch Ministries of Research and Education as well as Economic Affairs for funding the research.